

QCD corrections to charged current processes at the Next Linear Collider: CC10, CC11 and CC20 at $\mathcal{O}(\alpha_s)$.¹

Ezio Maina^a, Roberto Pittau^b and Marco Pizzio^a

^a*Dip. di Fisica Teorica, Università di Torino and INFN, Sezione di Torino, v. Giuria 1, 10125 Torino, Italy.*

^b*Paul Scherrer Institute
CH-5232 Villigen-PSI, Switzerland*

Abstract

One-loop QCD corrections to the full gauge invariant set of electroweak diagrams describing the charged current processes $e^+e^- \rightarrow u \bar{d} \mu \bar{\nu}_\mu$ (CC10), $e^+e^- \rightarrow u \bar{d} e^- \bar{\nu}_e$ (CC20) and $e^+e^- \rightarrow u \bar{d} s \bar{c}$ (CC11) are computed. We compare the exact calculation with a “naive” approach to strong radiative corrections which has been widely used in the literature and discuss the phenomenological relevance of QCD corrections for NLC physics.

¹ Work supported in part by Ministero dell' Università e della Ricerca Scientifica.

Introduction

The measurement of W mass to high precision is one of the goals of the NLC and will provide a stringent test of the Standard Model (SM) [1, 2]. In fact, the mass of the W boson in the SM is tightly constrained and an indirect determination of M_W can be obtained from a global fit of all present electroweak data. The fit gives [3] $M_W = 80.338 \pm 0.040_{-0.018}^{+0.009}$ GeV where the central value corresponds to $M_H = 300$ GeV and the second error reflects the change of M_W when the Higgs mass is varied between 60 and 1000 GeV. A disagreement between the value of M_W derived from the global fit and the value extracted from direct measurement would represent a major failure of the SM. The NLC is expected to reduce the error on the measurement of W mass down to about 15 MeV [4], to be compared with an error, assuming design luminosity, of about 50 MeV at Lep 2.

In order to extract the desired information from WW production data, theoretical predictions with uncertainties smaller than those which are foreseen in the experiments are necessary. This requires a careful study of all radiative corrections which have to be brought under control. In this note we will be concerned with QCD corrections which are known [5, 6] to modify the shape of the W -mass peak and the distributions of others kinematical variables. Since event shape variables are often used to extract WW production from the background it is highly desirable to have a complete next-to-leading order (NLO) study of these distributions for WW events. Furthermore, calculations of QCD corrections to $\mathcal{O}(\alpha^2\alpha_s^2)$ four-jet production have recently appeared [7]. Combining these results with a complete calculation of QCD corrections to all $\mathcal{O}(\alpha^4)$ four-fermion processes it would be possible to obtain NLO predictions for any four-jet shape variable at the NLC providing new means of testing perturbative QCD.

In this contribution we present the complete calculation of QCD corrections to $e^+e^- \rightarrow u \bar{d} \mu \bar{\nu}_\mu$, $e^+e^- \rightarrow u \bar{d} e \bar{\nu}_e$ and $e^+e^- \rightarrow u \bar{d} s \bar{c}$. While this is only a first step in the calculation of all $\mathcal{O}(\alpha^4)$ four-fermion processes at NLO, these reactions include the most important source of background, namely single W production, providing a natural setting for a first study of the role of QCD corrections to gauge invariant sets of four-fermion production diagrams. A gauge invariant description of $e^+e^- \rightarrow u \bar{d} s \bar{c}$ requires in the unitary gauge the eleven diagrams shown in fig. 1. This amplitude is known as CC11 in the literature. The subset of three diagrams labeled (e) and (f) in fig. 1, in which both W 's can go on mass-shell, is known as CC03 and is often used for quick estimates of WW production. The ten diagrams required for $e^+e^- \rightarrow u \bar{d} \mu \bar{\nu}_\mu$ (CC10) and the twenty diagrams required for $e^+e^- \rightarrow u \bar{d} e \bar{\nu}_e$ (CC20) are similar and can be readily deduced from our figures.

In most instances QCD corrections have been included “naively” with the substitution $\Gamma_W \rightarrow \Gamma_W(1 + 2/3 \alpha_s/\pi)$ and multiplying the hadronic branching ratio by $(1 + \alpha_s/\pi)$. This prescription is exact for CC03 when fully inclusive quantities are computed. However it can only be taken as an order of magnitude estimate even for CC03 in the presence of cuts on jet properties, as discussed in [5]².

² The impact of QCD corrections on the angular distribution of the decay products of a W and their application to on-shell W -pair production is discussed in ref.[8]

It is well known that differential distributions can be more sensitive to higher order corrections than total cross-sections in which virtual and real contributions tend to cancel to a large degree. It is therefore necessary to include higher order QCD effects into the predictions for WW production and decay in a way which allows to impose realistic cuts on the structure of the observed events.

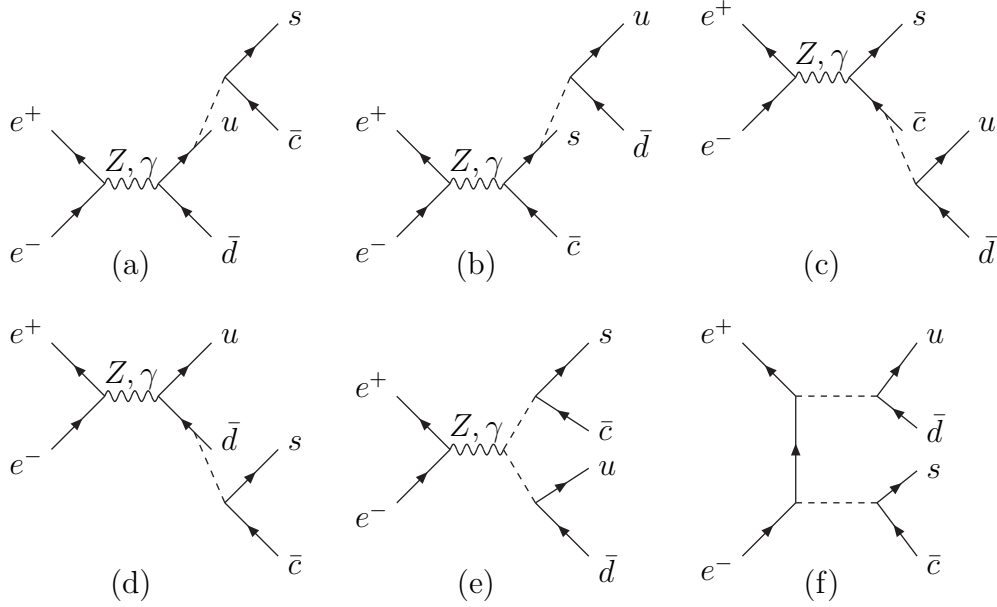


Figure 1: Tree level diagrams for $e^+e^- \rightarrow u \bar{d} s \bar{c}$. The dashed lines are W 's.

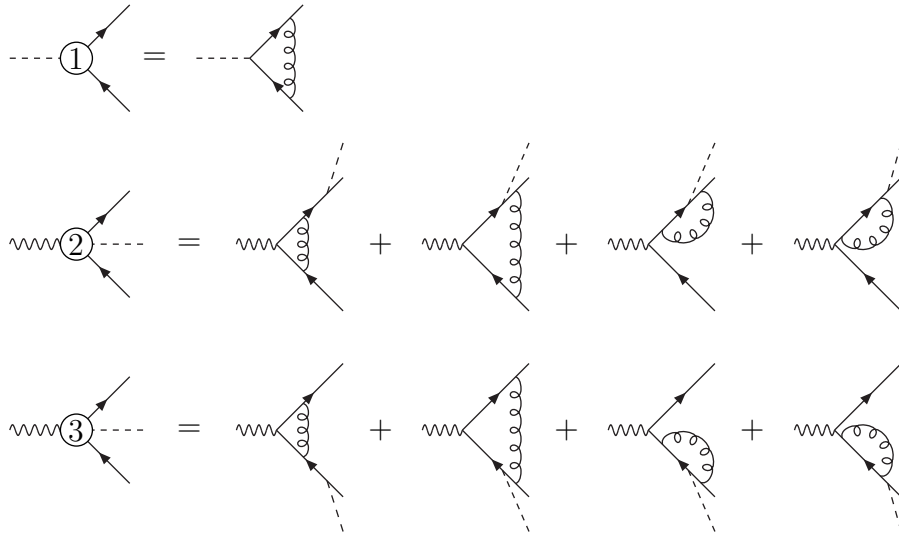


Figure 2: Basic combinations of loop diagrams. All virtual QCD corrections to electroweak four fermion processes can be computed using these three sets. The quark wave function corrections are not included because they vanish, in the massless limit, using dimensional regularization.

Calculation

One-loop virtual QCD corrections are obtained by dressing all tree diagrams with gluon loops. Defining suitable combinations of diagrams as in fig. 2 one can organize all contributions in a very modular way, as shown in fig. 3. As already mentioned in [6] all QCD virtual corrections to $\mathcal{O}(\alpha^4)$ four-fermion processes can be computed using the set of loop diagrams shown in fig. 2.

The real emission contribution can be obtained attaching a gluon to the quark line(s) of the tree diagrams in all possible positions. The required matrix elements have been computed using the formalism presented in ref. [9] with the help of a set of routines (PHACT) [10] which generate the building blocks of the helicity amplitudes semi-automatically.

The calculation of the virtual corrections has been performed in two different ways, with identical results. In the first case we have used the standard Passarino–Veltman [11] reduction procedure, while in the second we have used the new techniques presented in [12].

In order to be able to integrate separately the real and virtual part one has to explicitly cancel all singular contributions in each term in a consistent way. To this aim we have used the subtraction method. Benefits of this method are twofold. First, an exact result is obtained and no approximation needs to be taken; second, all singular terms are canceled under the integration sign and not at the end of the calculation, leading to better numerical accuracies. This is especially relevant for the present case, since we are aiming for high precision results, with errors of the order of a per mil. We have found it particularly convenient to implement the dipole formulæ of reference [13]. These are a set of completely general factorization expressions which interpolate smoothly between the soft eikonal factors and the collinear Altarelli–Parisi kernels in a Lorentz covariant way, hence avoiding any problem of double counting in the region in which partons are both soft and collinear.

All integrations have been carried out using the Monte Carlo routine VEGAS [14].

In the absence of a calculation of all $\mathcal{O}(\alpha)$ corrections to four-fermion processes, we have only included the leading logarithmic part of ISR using the β prescription in the structure functions, where $\beta = \ln(s/m^2) - 1$. Beamstrahlung effects have been ignored.

Results

In this section we present a number of cross sections and of distributions at $\sqrt{s} = 500$ GeV. We have used $\alpha_s = .123$ in order to conform to the choice made for the Joint ECFA/DESY Study. Initial state radiation is included in all results.

For the NLC workshop the so called NLC/TH set of cuts have been agreed on:

- the energy of a jet must be greater than 3 GeV;
- two jets are resolved if their invariant mass is larger than 10 GeV;
- jets can be detected if they make an angle of at least 5° with either beam.

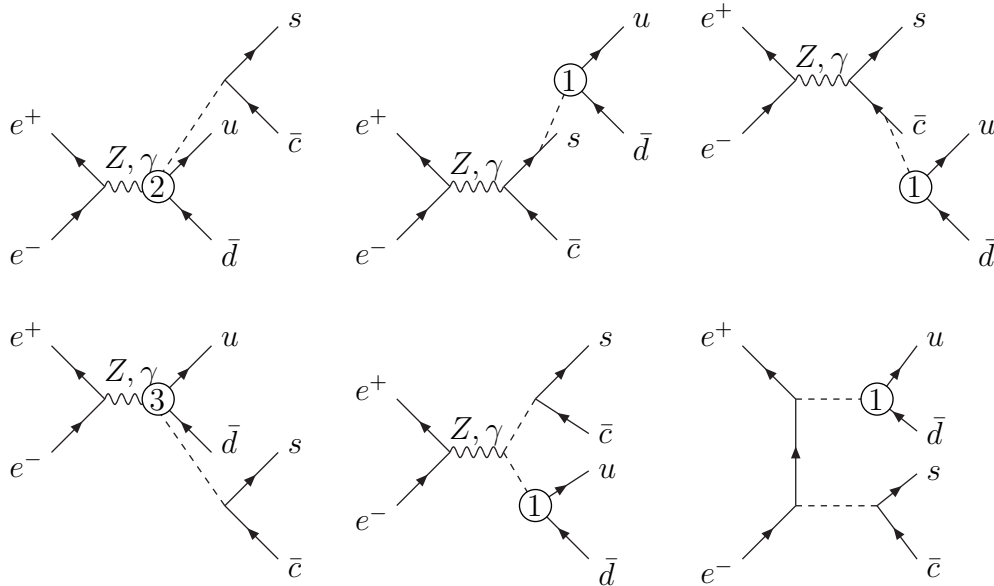


Figure 3: One loop gluonic corrections to the $u \bar{d}$ line of the $e^+e^- \rightarrow u \bar{d} s \bar{c}$ process. Similar corrections on the $s \bar{c}$ line must be included.

This set of cuts will be referred to as “canonical” in the following. We have preferred a different criterion for defining jets which is closer to the actual practice of the experimental collaborations. For mass reconstruction studies we have used the Durham [15] scheme with $y_D = 1. \times 10^{-3}$. The four-momenta of the particles which have to be recombined have been simply summed. If any surviving jet had an energy smaller than 3 GeV it was merged with the jet closest in the Durham metric.

Previous studies [16] have shown that the differences between the total cross sections obtained from CC10 and CC11 and those obtained with CC03 are at the per mil level. The non resonant background is far more important when there is an electron in the final state: the cross section, with canonical cuts, for CC20 at $\sqrt{s} = 190$ GeV is larger than the cross section calculated from CC03 by several percent. When the full NLO results is compared with the naive-QCD (nQCD) predictions, large effects have been found in observables like the average shift of the mass reconstructed from the decay products from the true W mass for fully hadronic processes.

In fig. 4 and 5 we show some representative distribution for the semileptonic events. In fig. 4a we present the normalized distribution of the angle between the muon and the closest jet for CC10. The events in fig. 4a pass all NLC/TH cut with the exception of the minimum $\theta_{\mu j}$. With increasing collider energy, the two W ’s tend to fly apart with larger relative momentum and therefore the probability of a jet to overlap with the lepton decreases. This behaviour is clearly visible in fig. 4a which shows that jets are typically well separated in angle from the charged lepton and that the differences between the exact distribution and the one with “naive” corrections is confined to very large angles.

Fig. 4b shows the distribution of the minimum angle between any jet and either beam. We have separated the contribution of two-jet and three-jet final states making

it possible to estimate the effect of different angular cuts on the cross section.

The total NLO cross section with canonical cuts is $.23554(4)$ pb , to be compared with the nQCD results of $.23065(3)$. The two predictions differ by more than 2%.

Fig. 5a and 5b present the normalized distributions of the angle between the electron and the closest jet and of the minimum angle between any jet and either beam, respectively, for $e^+e^- \rightarrow u \bar{d} e \bar{\nu}_e$.

In fig. 6 we compare the NLO spectrum of the average reconstructed W mass for CC11 with the nQCD case result. All events with at least four observed jets have been retained in the plots. The two candidate masses are obtained forcing all events to four jets, merging the two partons which are closest in the Durham scheme, and then selecting the two pairs which minimize

$$\Delta'_M = (M_{R1} - M_W)^2 + (M_{R2} - M_W)^2. \quad (1)$$

where M_{R1} M_{R2} are the two candidate reconstructed masses and M_W is the input W mass. In fig. 6 the dashed line refers to the nQCD results while those of the full NLO calculation are given by the continuous line. Our plot is obtained using only the basic set of cuts described above.

Fig. 6 shows that at NLO the mass distribution is shifted towards lower masses and a long tail for rather small average masses is generated. Because of the larger relative momentum of the two W 's it is less likely that partons from the decay of one W end up close to the decay products of the other W -boson, therefore the effect is smaller than at Lep 2 energies [17].

In fig. 7 we present the distributions of the following four-jet shape variables [18]:

- the Bengtsson-Zerwas angle: $\chi_{BZ} = \angle[(\mathbf{p}_1 \times \mathbf{p}_2), (\mathbf{p}_3 \times \mathbf{p}_4)]$ (fig. 7a);
- the Körner-Schierholz-Willrodt angle :
 $\Phi_{KSW} = 1/2\{\angle[(\mathbf{p}_1 \times \mathbf{p}_4), (\mathbf{p}_2 \times \mathbf{p}_3)] + \angle[(\mathbf{p}_1 \times \mathbf{p}_3), (\mathbf{p}_2 \times \mathbf{p}_4)]\}$ (fig. 7b);
- the angle between the two least energetic jets; $\alpha_{34} = \angle[\mathbf{p}_3, \mathbf{p}_4]$ (fig. 7c);
- the (modified) Nachtmann-Reiter angle: $\theta_{NR}^* = \angle[(\mathbf{p}_1 - \mathbf{p}_2), (\mathbf{p}_3 - \mathbf{p}_4)]$ (fig. 7d).

The numbering $i = 1 \dots, 4$ of the jet momenta \mathbf{p}_i corresponds to energy-ordered four-jet configurations ($E_1 > E_2 > E_3 > E_4$). We compare the exact NLO results with the distributions obtained in nQCD and with the results obtained at tree level from the standard background reactions $e^+e^- \rightarrow q \bar{q} g g$ and $e^+e^- \rightarrow q_1 \bar{q}_1 q_2 \bar{q}_2$.

In all subplots of fig. 7 the full NLO results are given by the continuous line and the nQCD prediction is given by the dashed line. The $q \bar{q} g g$ and $q_1 \bar{q}_1 q_2 \bar{q}_2$ tree level background distributions are given by the chain-dotted and the dotted line respectively. The shape variables are computed following the procedure outlined in ref. [19] where the Durham cluster algorithm is complemented by the E0 recombination scheme, namely if the two particles i and j are merged the pseudo-particle which takes their place remains massless, with four-momentum:

$$E_{new} = E_i + E_j, \quad \mathbf{p}_{new} = \frac{E_i + E_j}{|\mathbf{p}_i + \mathbf{p}_j|}(\mathbf{p}_i + \mathbf{p}_j). \quad (2)$$

Using this clustering procedure all five-jet events are converted into four-jet events, then each event is used in the analysis if $\min_{i,j=1,4} y_{ij} > y_{cut}$ with $y_{cut} = 0.001$. In particular no minimum angle between jets and either beams is required.

It should be stressed that four-jet shape variables in WW events measure the correlations between the hadronic decays of the two W 's and therefore it should be explicitly checked whether existing codes, NLO calculations or parton shower Monte Carlo programs, successfully reproduce the experimental curves.

A separation based on shape-variables of WW events from the background seems, at first sight, to be rather difficult at the NLC. The variable which most clearly discriminates between signal and background is the angle between the two least energetic jets α_{34} . While the signal distribution peaks in the backward direction the background is almost flat. On the contrary, the Bengtsson-Zerwas angle and the Körner-Schierholz-Willrodt angle distribution from CC11 are almost indistinguishable from those generated from the $q \bar{q} g g$ background. Some additional sensitivity is provided by the Nachtmann-Reiter angle distribution. Both signal and background peak at small angles, but while the former is almost negligible in the backward direction, the latter shows a large tail which extends to 180° . The distributions obtained in nQCD are very similar to the full NLO results, contrary to what happens at lower energies [17].

Conclusions

We have described the complete calculation of QCD radiative corrections to the charged current processes $e^+e^- \rightarrow u \bar{d} \mu \bar{\nu}_\mu$, $e^+e^- \rightarrow u \bar{d} e \bar{\nu}_e$ and $e^+e^- \rightarrow u \bar{d} s \bar{c}$ which are essential in order to obtain theoretical predictions for W -pair production with per mil accuracy. The amplitudes we have derived are completely differential, and realistic cuts can be imposed on the parton level structure of the observed events. For CC11 we have presented the distribution of the average reconstructed W mass in fully hadronic events and the distribution of several four-jet shape variables. For CC10 and CC20 the distributions obtained in nQCD are very similar to the exact NLO results, however the corresponding total cross sections can differ by more than 2%.

References

- [1] The most complete review of W -pair production at Lep 2 can be found in the Proceedings of the Workshop on Physics at Lep 2, G. Altarelli, T. Sjöstrand and F. Zwirner eds., Cern 96-01.
- [2] A. Ballestrero *et al.*, Determination of the mass of the W boson, in ref.[1], Vol. 1, p. 141.
- [3] The LEP Electroweak Working Group and the SLD Heavy Flavour Group, LEPEWWG/96-02.
- [4] E. Accomando *et al.*, DESY 97-100, hep-ph/9705442.
- [5] E. Maina and M. Pizzio, Phys. Lett. **B369** (1996) 341.
- [6] E. Maina, R. Pittau and M. Pizzio, Phys. Lett. **B393** (1997) 445.
- [7] J.M. Campbell, E.W.N. Glover and D.J. Miller, hep-ph/9706297;
E.W.N. Glover and D.J. Miller, hep-ph/9609474;
Z. Bern, L. Dixon, D.A. Kosower and S. Weinzierl, hep-ph/9609460;
A. Signer and L. Dixon, hep-ph/9609460;
A. Signer and L. Dixon, hep-ph/9706285;
Z. Nagy and Z. Trócsányi, hep-ph/9707309.
- [8] K.J. Abraham and B. Lampe, *Nucl. Phys.* **B 478** (1996) 507.
- [9] A. Ballestrero and E. Maina, Phys. Lett. **B350** (1995) 225.
- [10] A. Ballestrero, in preparation.
- [11] G. Passarino and M. Veltman, *Nucl. Phys.* **B 160** (1979) 151.
- [12] R. Pittau, PSI-PR-96-19, hep-ph/9607309, to be published in *Comp. Phys. Comm.*
- [13] S. Catani and M.H. Seymour, *Nucl. Phys.* **B 485** (1997) 291.
- [14] G.P. Lepage, Jour. Comp. Phys. **27** (1978) 192.
- [15] N. Brown and W.J. Stirling, Phys. Lett. **B252** (1990) 657; Z. Phys. **C 53** (1992) 629.
- [16] E. Accomando *et al.*, Event generators for WW physics, in ref.[1], Vol. 2, p. 3.
- [17] E. Maina, R. Pittau and M. Pizzio, DFTT 47/97, PSI-PR-97-18.

- [18] J.G. Körner, G. Schierholz and J. Willrodt, *Nucl. Phys.* **B185** (1981) 365;
O. Nachtmann and A. Reiter, *Z. Phys.* **C16** (1982) 45;
M. Bengtsson and P.M. Zerwas, *Phys. Lett.* **B208** (1988) 306;
M. Bengtsson, *Z. Phys.* **C42** (1989) 75;
S. Betke, A. Richter and P.M. Zerwas, *Z. Phys.* **C49** (1991) 59.
- [19] R. Barate *et al.*, ALEPH Coll., CERN-PPE/97-002.

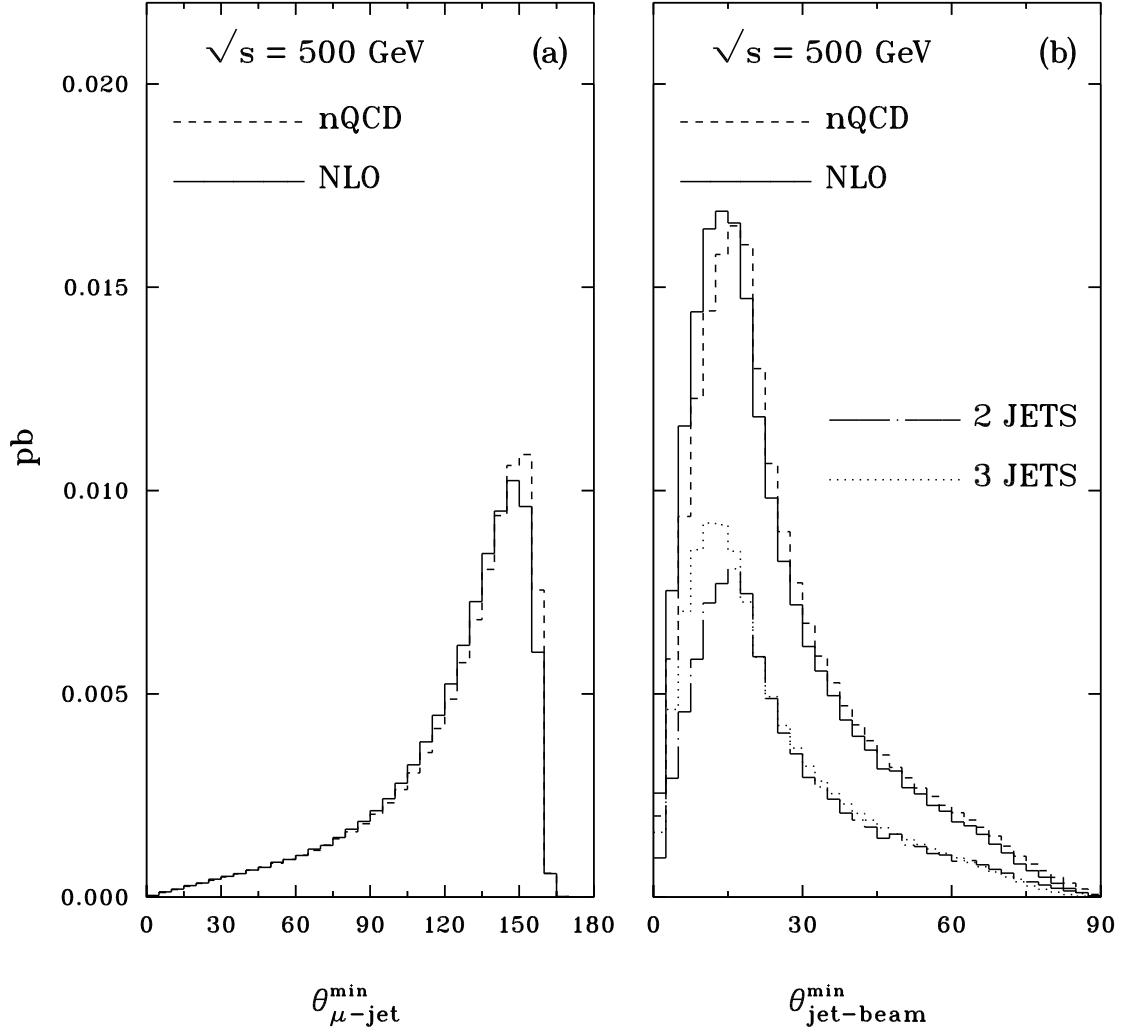


Fig. 4: Distribution of the angular separation of the μ^- from the closest jet (a) and of the minimum angular separation between any jet and either beam (b) at $\sqrt{s} = 500$ GeV for CC10. The continuous, dotted and dot-dashed histograms are exact NLO results while the dashed histogram refers to nQCD.

$\sqrt{s} = 500 \text{ GeV}$ CC20 NLC/TH

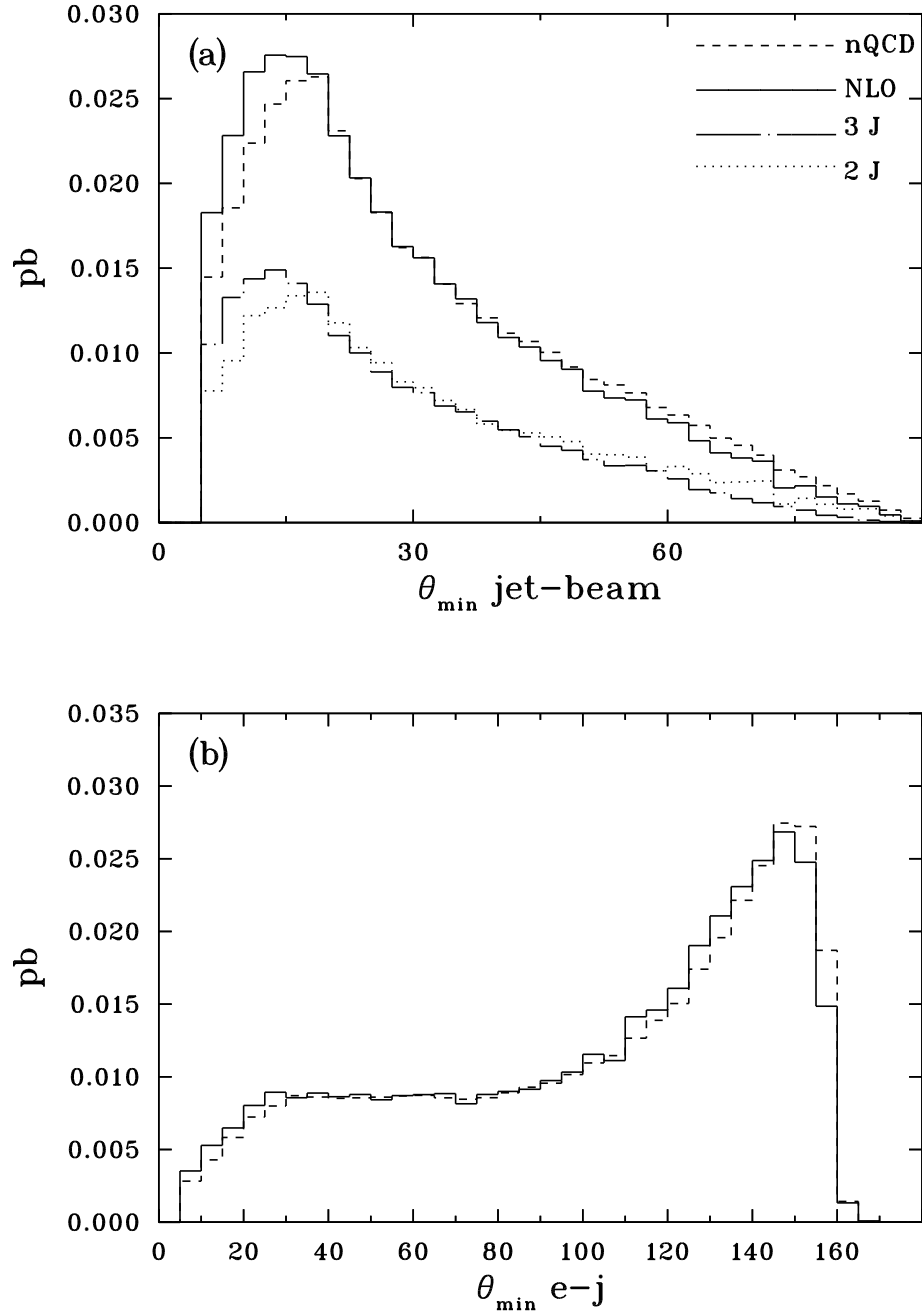


Fig. 5: Angular separation of the e^- from the closest jet (a) and between any jet and either beam (b) at $\sqrt{s} = 500 \text{ GeV}$. The continuous, dotted and dot-dashed histograms are exact NLO results while the dashed histogram refers to nQCD.

$\sqrt{s} = 500 \text{ GeV}$ CC11 ISR NLC/TH DURHAM

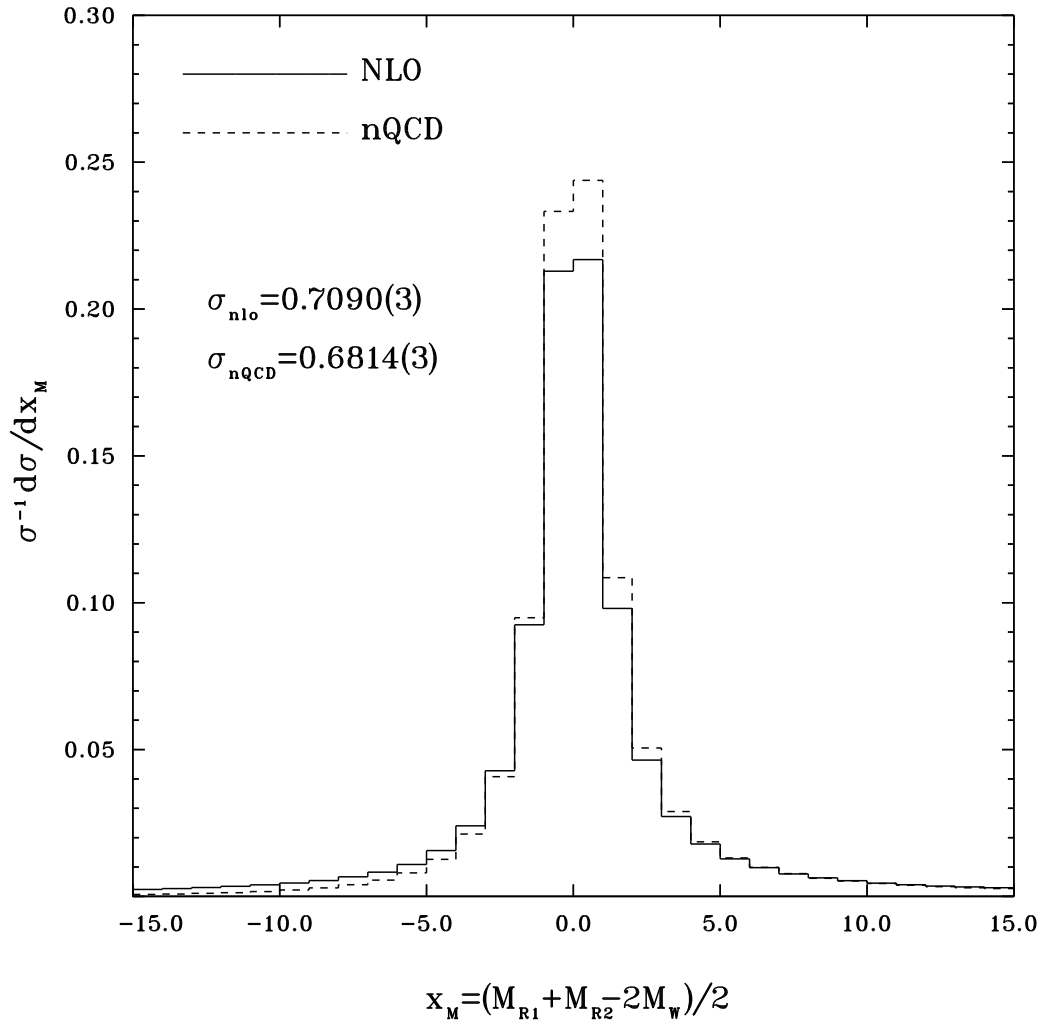


Fig. 6: Average mass distribution at $\sqrt{s} = 500 \text{ GeV}$. All NLC/TH cuts are applied. The continuous histogram is the exact NLO result while the dashed histogram refers to nQCD.

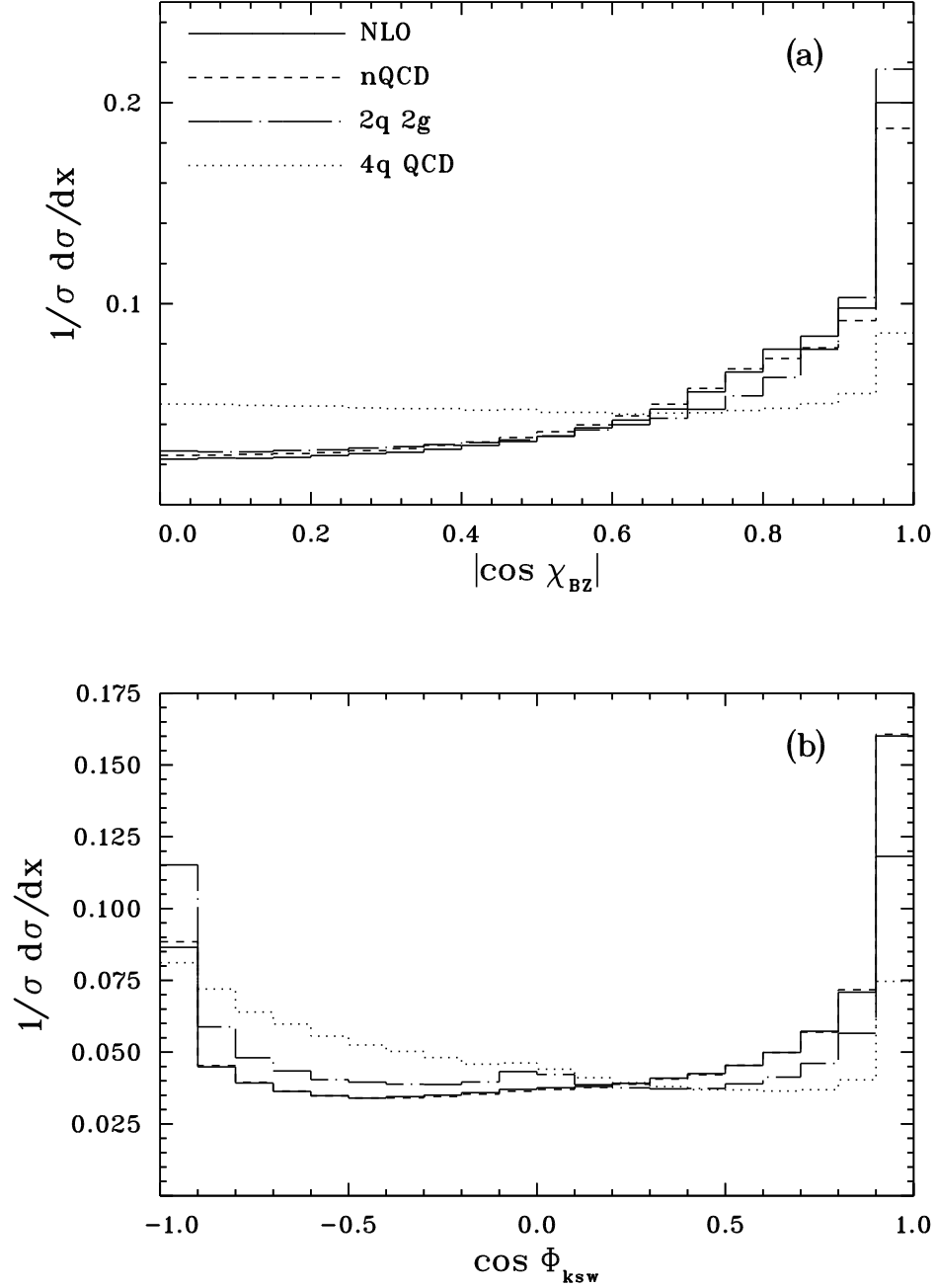


Fig. 7: Four-jet shape variables at $\sqrt{s} = 500$ GeV. The full NLO results (continuous line) is compared with the nQCD prediction (dashed line) and with the tree level background distributions from $q \bar{q} g g$ (chain-dotted line) and $q_1 \bar{q}_1 q_2 \bar{q}_2$ (dotted line).

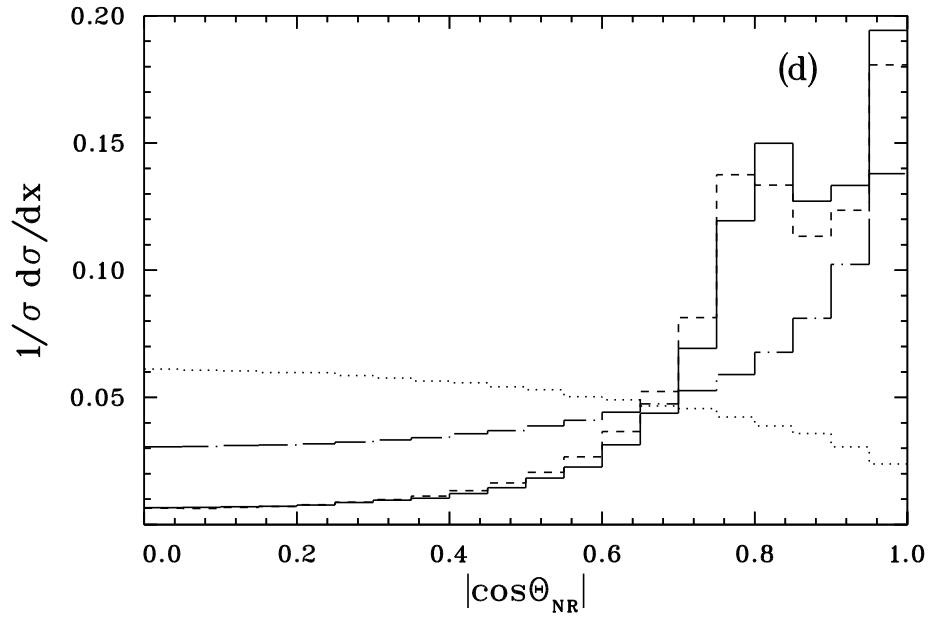
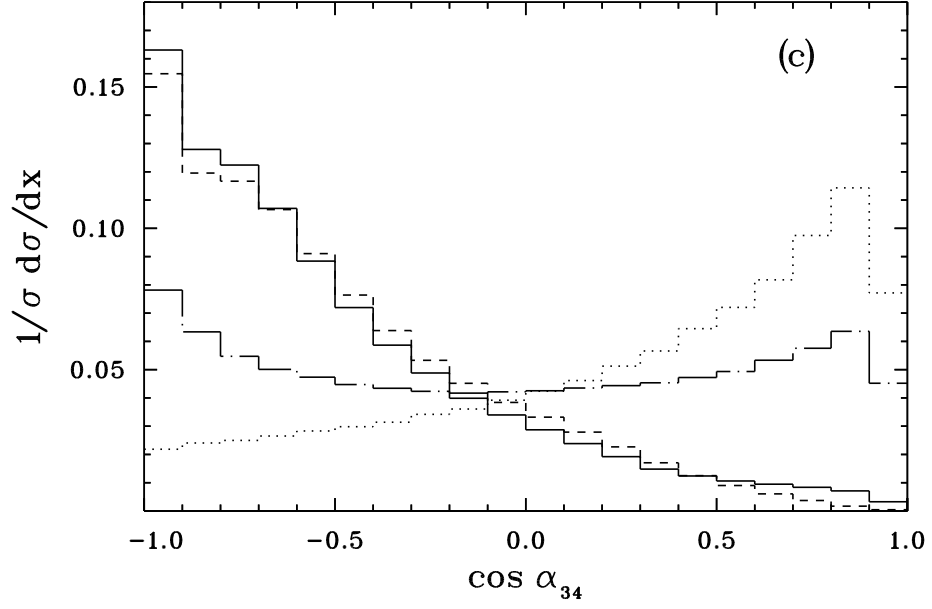


Fig. 7: Four-jet shape variables at $\sqrt{s} = 500$ GeV, continued.